LUND UNIVERSITY
Faculty of Science

DMI
Vejr, klima og hav

ANALYZING METEOROLOGICAL RELATIONSHIPS TO AEROSOLS IN CHINA

Carl Svenhag
Bachelor's Thesis

Supervisors:
Kristian Pagh Nielsen & Elna Heimdal Nilsson

Danish Meteorological institute
Lund University, Department of Physics
May 2017

Carl.svenhag.699@student.lu.se

Abstract

Meteorological conditions are influenced everyday by air-bound aerosols and pollution in the atmosphere, and understanding these processes from micro to synoptic scale, is essential for forecasting and creating high resolution weather models. In this study, three different experimental weather models are analysed to provide some understanding on how various meteorological parameters are influenced by modelling atmospheric aerosols. Conclusions surrounding relations between the individual parameters are drawn from the results and discussed with respect to previous studies and knowledge on meteorology and atmospheric chemistry.

This analytic observation was made from data covering the Chinese Yangtze River Delta region over the months January and July 2010. This region holds the metropolitan city of Shanghai and experiences a relative subtropical monsoon climate.

Examining how the direct and indirect climate effects influence weather parameters through the three simulated experimental models, attempting to draw conclusions connecting aerosol characteristics to the dynamics of the atmosphere. The primarily investigated parameters include surface temperature, cloud cover, precipitation in the form of rain, long and shortwave radiation measured near surface and at top of atmosphere. Differences in solid precipitation between the experiments are very small and will not be covered in this analytic study.

Highlighting the relation between certain simulated parameters with respect to urban aerosols for additional observation concerning the climate effects.

Furthermore, a modest investigation of a special case day scenario is analyzed to observe how short-term forecasting could be influenced by simulated aerosol modelling in hourly depict data.

Acknowledgements

This research was performed under the supervision of Kristian Pagh Nielsen at Danske Meteorologiske Institut (DMI) who provided great help during my project. I am grateful for all the background material and articles he presented me during my bachelor project and additionally helping me understand the operating system of Linux and the Gnuplot software. I am certain these provided skills will come to help me in my future studies and I am grateful for the opportunity to access research material and supervision at DMI.

I would also like to thank Elna Heimdal Nilsson at Lund University for her support and guidance during my bachelor work and throughout my three years at Lund University.

This thesis is an individual extension of the Marco Polo (2014-2017) project at DMI, which is "Monitoring and Assessment of Regional air quality in China using space Observations, Project Of Long-term sino-european co-Operation". This implies that papers on similar outcome and research could be found in future publications.

Contents

Acronyms

DMI	**D**anske **M**eteorologiske **I**nstitut
YRD	**Y**angtze **R**iver **D**elta
HARMONIE	**H**IRLAM-**A**LADIN **R**esearch for **M**esoscale **O**perational **N**umerical **W**eather **P**rediction in **E**uromed
HIRLAM	**H**igh **R**esolution **L**imited **A**rea **M**odel
ALADIN	**A**ire **L**imitee **A**daptation dynamique **D**eveloppement **I**nternational
IFS	**I**ntegrated **F**orecast **S**ystem
CC	**C**loud **C**over
AOD	**A**erosol **O**ptical **D**epth
CCN	**C**loud **C**ondensation **N**uclei
CDNC	**C**loud **D**roplet **N**umber **C**oncentration
NWP	**N**umerical **W**eather **P**rediction
CAPE	**C**onvective **A**vailable **P**otential **E**nerergy

Introduction

The massive economic growth of China over last decades have led to a huge dependence on coal burning and transportation by combustion of fossil fuel. These processes exhausts millions of particles into the lower troposphere and these particles can be carried away distances extending over the Pacific Ocean and ascending through the lower stratosphere. However, the Chinese megacities producing these anthropogenic aerosols are the ones confronting the most hazardous concentrations of particulate matter (PM), with air quality levels considered to be severely unhealthy in some urban areas. This abundant increase of larger aerosols into the atmosphere is bound to have some climate effect as well, ramifications that could perturbate the atmospheric balance forcing further cooling or warming to the environment depending on characteristics of the emitted pollution.

The atmosphere is experiencing both direct and indirect climate effects associated with characteristics of the air-bound aerosols. By simulating experimental models which implement the two climate effects, generating distinctive result for various weather parameters, one could partially describe the relationship between aerosol particles and atmospheric mechanisms. A Cooperation between European meteorological institutes have created an operational non-hydrostatic weather model called HARMONIE, able to perform weather-data simulations over eastern Asia, which was used as basis and reference for our cases during this analytic study over the YRD region in China.

The incoming and outgoing short and longwave radiation gives some description of the aerosols climate effect, and by studying cloud cover variations and precipitation one could portray how aerosols possibly supplement large-scale droughts and other meteorological phenomena's, which also could be useful for related climate and weather forecasting studies. Aerosols relation to radiation from the Sun and climate is described by the mentioned direct and indirect effect, and by analysing both winter and summer seasonal data over a highly populated area in China, you can observe and analyse how important changes in model urban aerosol dynamics could significantly change the accuracy of a forecast.

2. **Background**

2.1 Aerosols Atmospheric Effects

There are considerable amounts of physical processes occurring in the atmosphere, from small micro-scale systems to large synoptic circulations. The certain correlation air-bound particles have with radiation the climate is one of many altering factors, and understanding their mechanisms can help interpret the dynamics of the atmosphere.

As the shortwave solar radiation enters our atmosphere it immediately begins to interact with the present aerosols, scattering and absorbing the radiation. When the particle absorbs radiation, it must release energy by applying heat to its surrounding environment. As this could lead to a local temperature increase, by containing high concentrations of absorbing aerosols, the region is then experiencing a warming direct climate effect and possible radiative forcing. High concentrations of soot and Black Carbon are shown to have this positive radiative forcing effect (Boucher 2006). A case of direct cooling effects e.g. occurs when the highly concentrated aerosols have efficient scattering characteristic of shortwave solar radiation. This prevents energy (heat) to reach lower altitudes implying negative radiative forcing and resulting in cooling of its surrounding atmosphere. Additional information concerning radiative forcing given in Ahrens (2008).

To characterize which of these processes the aerosol will undergo for a certain wavelength, the aerosol optical depth (AOD) gives a description of the radiation-aerosol interaction. A detailed explanation of AOD is given in Thomas and Stamnes (1999).

Clouds are also known to include absorbing and reflecting capability on solar radiation, with a varying single scattering albedo depending on cloud type. Twomey (1959) gives a description of how aerosols influence the formation of clouds, illustrating how the indirect climate effect occurs when aerosols act as cloud condensation nuclei to form additional cloud droplets, thereby increasing the overall cloud cover. Furthermore, Twomey (1977) explains how certain anthropogenic aerosols produce clouds which scatter solar radiation more efficiently than regular ones, also how this could generate smaller cloud droplets which prevents formation of precipitation. This is due to gravity not overcoming the buoyancy of the smaller cloud droplet and thereby forcing it to remain aloft. This could be insightful when observing the experimental models simulated rainfall in our analysis with and without Twomey's indirect effect included.

The cloud-lifetime effect, or Albrecht effect, also adds that possible anthropogenic aerosols, acting as cloud condensation nuclei (CCN), generating clouds with longer lifetime which may decrease the total amount of shortwave radiation reaching the surface during overcast, and so resulting in cooling of the lower troposphere (Albrecht 1989).

Absorption by aerosols in the atmosphere may also cause clouds to influence the vertical temperature profile, determining the atmospheric stability, described as the semi-direct effect. For example, producing surface cooling and atmospheric heating creates a vertically stable atmosphere, this environmental condition produces no convective available potential energy (CAPE) and prohibits convective formation of clouds, this could bring about a dryer environment with calmer weather. Further explanation of this phenomenon is made by Fan et al. (2008).

2.2 Aerosol Modelling Studies

Inquiry to improve the accuracy of weather forecasts has been developing since Carl-Gustav Rossby and a group of meteorologists in Stockholm assembled the first operational weather model in 1954. However, even if the numerical weather predictions (NWP) we use today are digitized and significantly more advanced, we still lack the modelling proficiency to produce flawless forecasts of weather and climate over a longer period.

Additional research on how anthropogenic and naturally occurring aerosols influence weather models could improve their accuracy for the future. Toll et al. 2015 studied how the HARMONIE model perceives solar radiation due to this aerosol effect. Their study includes how aerosols in forest-fire smoke over Russia reduced the amount of shortwave radiation reaching the surface. The increased thickness of aerosols in the study shares some insight to the analysed YRD area which has an atmosphere with average AOD 5 times the global average (Stier et al. 2005). These areas should be expected to experience greater consequences from the aerosol effects.

Radiative Forcing from the influence of aerosols in East-Asian climate has been investigated by Zhang et al. (2011). The research showed that the average temperature decreased with more than 0.5 degrees Celsius due to carbon and sulphate aerosols, and resulting in a decreased amount of precipitation falling over eastern Asia by 0.14 mm per day during summer months. Connecting with results from Bollasina et al. (2011) which concluded that the summer monsoon is weakening due to anthropogenic aerosols gives some background on the YRD region conditions to include in this analysis.

The mentioned aerosol-influenced semi-direct effect has been studied by Wang et al. (2012) over south-eastern China, with research covering a weekly cycle to observe a maximum and minimum occurrence of sulphate (SO_2) due to urban activity in relation to this climate effect. Their case showed small anomalies in cloud cover and humidity over the studied timeframe, but the study puts emphasis on necessary further investigation on the semi-direct effect from urban pollution and aerosols

Studies on the Chinese YRD domain, positioned on latitudes and altitudes 28.5–33.5◦ N and 117.5–123.5◦ E, show significantly high Black Carbon and sulphate emissions (Streets et al., 2001; Lu et al., 2010). Considering population density to be directly related to urban anthropogenic emissions, an approximate background map of urban-rural population (Figure 1.) could be used to analyze potential local similarities to simulated parameters over eastern China.

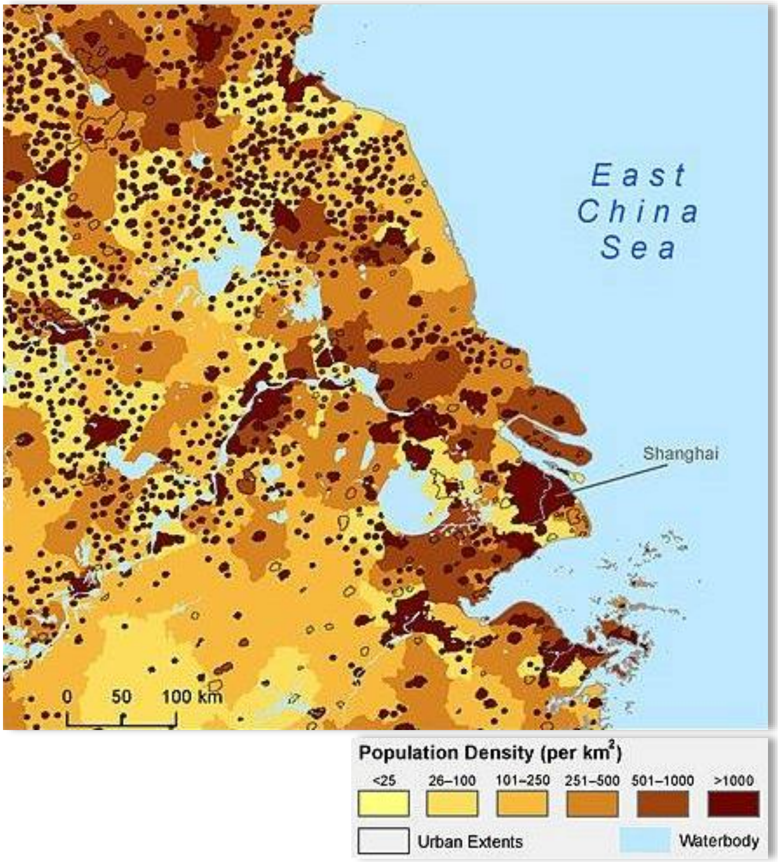

Figure 1. 2010 Estimated urban-rural population over near-Shanghai region in Eastern China with population density on a colour-scheme. Figure extracted from SEDAC (2013).

3. **Methodology**

During this analysis, the main tool for observing the YRD data over January and July 2010 is applied with the Gnuplot software through the Linux command terminal, primarily to plot figures and tables. The acquired data sets mainly consist of 15-minute time steps accumulated into six hour fixtures for each parameter on three simulated model experiment, stretching from UTC time-steps 00+6, 06+6, 12+6 and 18+6 hours, accounted that the YRD time zone is UTC/GMT+8h. These parameters are plotted on a two-dimensional colormap over the YRD region with a spatial resolution of 1^{o} in the datasets, designating each parameter with a certain colour-scheme to provide a satisfying observation. The produced script to plot this map is then attached with a data-scheme to produce an x and y axis realigned with latitudes and longitudes relative to Earth (see appendix). Hourly accumulated data is obtained as well to study specific cases.

Datasets of averaged land area mean results, also with 6-hour frequency, is additionally provided for plotting diagrams to observe and analyse relative differences between models and parameters.

3.1 Model Features

The acquired data sets were originally produced from the TERRA and AQUA satellites equipped with the MODIES instrument, this tool could analyze the relationship between AOD, CC and water vapor. Further studies on this is done by Kourtidis et al. (2015). The provided model experiments originate from a HARMONIE weather model cycle described by Bengtsson et al. (2017), and this high-resolution model is the one we use primarily at DMI.

The HARMONIE cycle is acting as a reference experimental model in this analytic study, this implements radiation physics generated through the integrated forecast system (IFS) cycle by ECMWF (2015). This includes a radiation scheme with cloud droplet number concentrations (CDNC) described by Martin et al. (1994), which was assumed to be constant over the whole YRD region covering both land and sea. The types of aerosols included in the IFS scheme covers land, sea, desert, urban, volcanic (stratosphere) and stratospheric background aerosols. Regarding the IFS climatology, it was considered that the model consists of AOD characteristics which has too low thickness compared to what is realistically believed to be present in the YRD region.

That is why the second aerosol experimental model, labelled the Direct Aerosol case, is included in the analysis to study the previous HARMONIE cycles with a reanalyzed AOD data set (MACC) from Inness et al. (2013). They were converted into IFS aerosol categories of land, sea, urban and desert types. This includes a more realistic AOD thickness and thereby implementing the direct climate effects on our analyzed parameters, describing simulated long and shortwave radiation's relation to AOD. The

MACC reanalysis also covers the mentioned semi-direct effect, possibly detecting the absorption within and surrounding clouds.

To include the indirect effect in our analysis, data sets acquired from the third experimental model, labelled the Total Aerosol case, is added. These simulated results are also run with the MACC aerosol replacements but is substituting the default constant CDNC assumption with Menon et al. (2002) parametrization to include the mentioned Twomey effect. This enables observation of the changes in cloud cover (CC) and accumulated rainfall due to this effect in addition to the change in AOD data.

4. Results and Discussion

The progression of our analytic process is produced in this section with selected figures for observation. Firstly, displaying the foregoing diagrams of the available parameters which directed the focus of our study, followed with an investigation of those specific parameters. The chosen parameters for evaluation were based on significant differences between the three experimental models, and motives to establish connections to previous studies in Section 2. The main analysed parameters are cloud cover, surface longwave (LW) and shortwave (SW) radiation, and these are illustrated in diagrams and maps bound with a special day case (see Section 4.2).

By plotting the daytime average MACC aerosol type concentrations, mentioned in Section 3.1, for January and July we obtain a basis outlook on high and low occurrence of the urban aerosols in Figure 2.

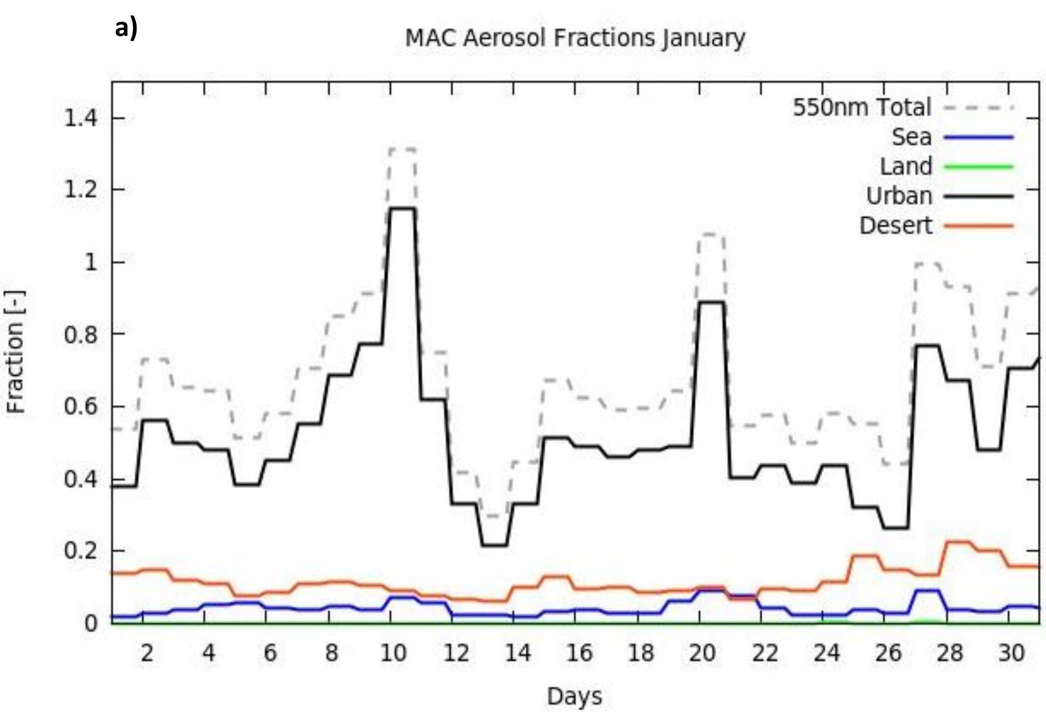

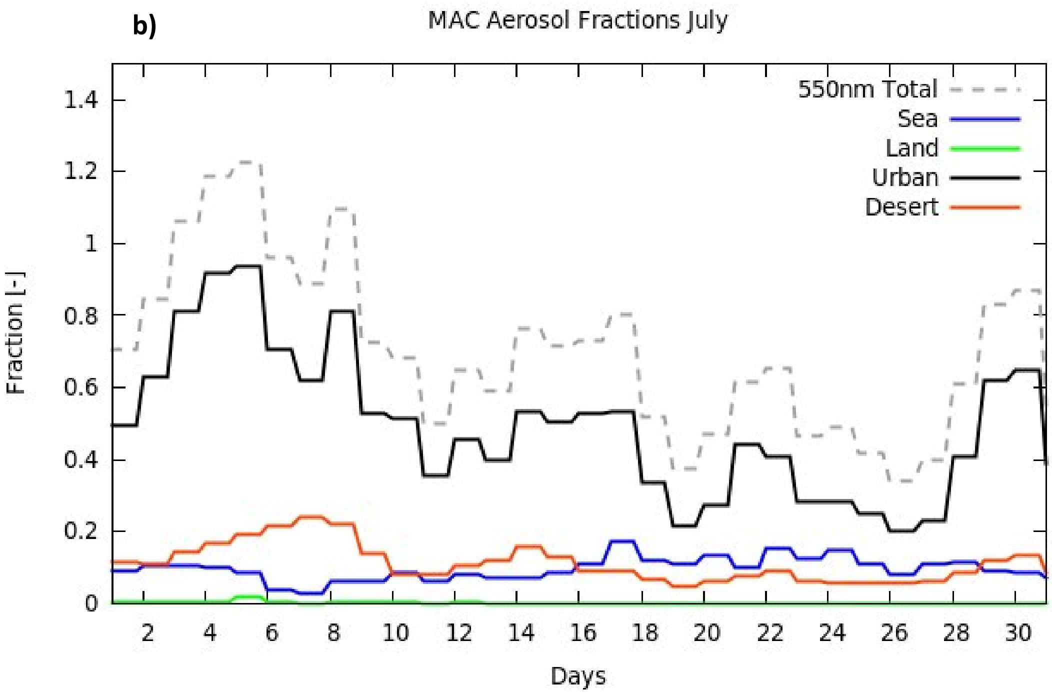

Figure 2. Average daytime MACC AOD fractions and types from January (**a)** and July (**b)** 2010 over the YRD domain. 550nm was the electromagnetic wavelength for the used AOD in the provided data, see section 2.1.

Then additionally, the reference model land area mean data for investigated parameters is plotted to get an overview of the overall meteorological conditions during the two months, this is also used to analyse mentioned distinguishable relationships between parameters and Figure 2a-b.

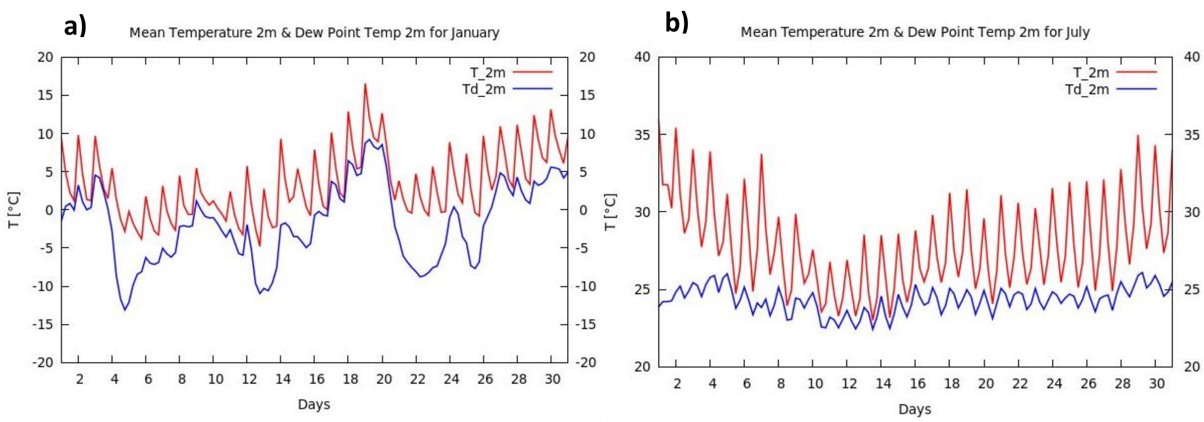

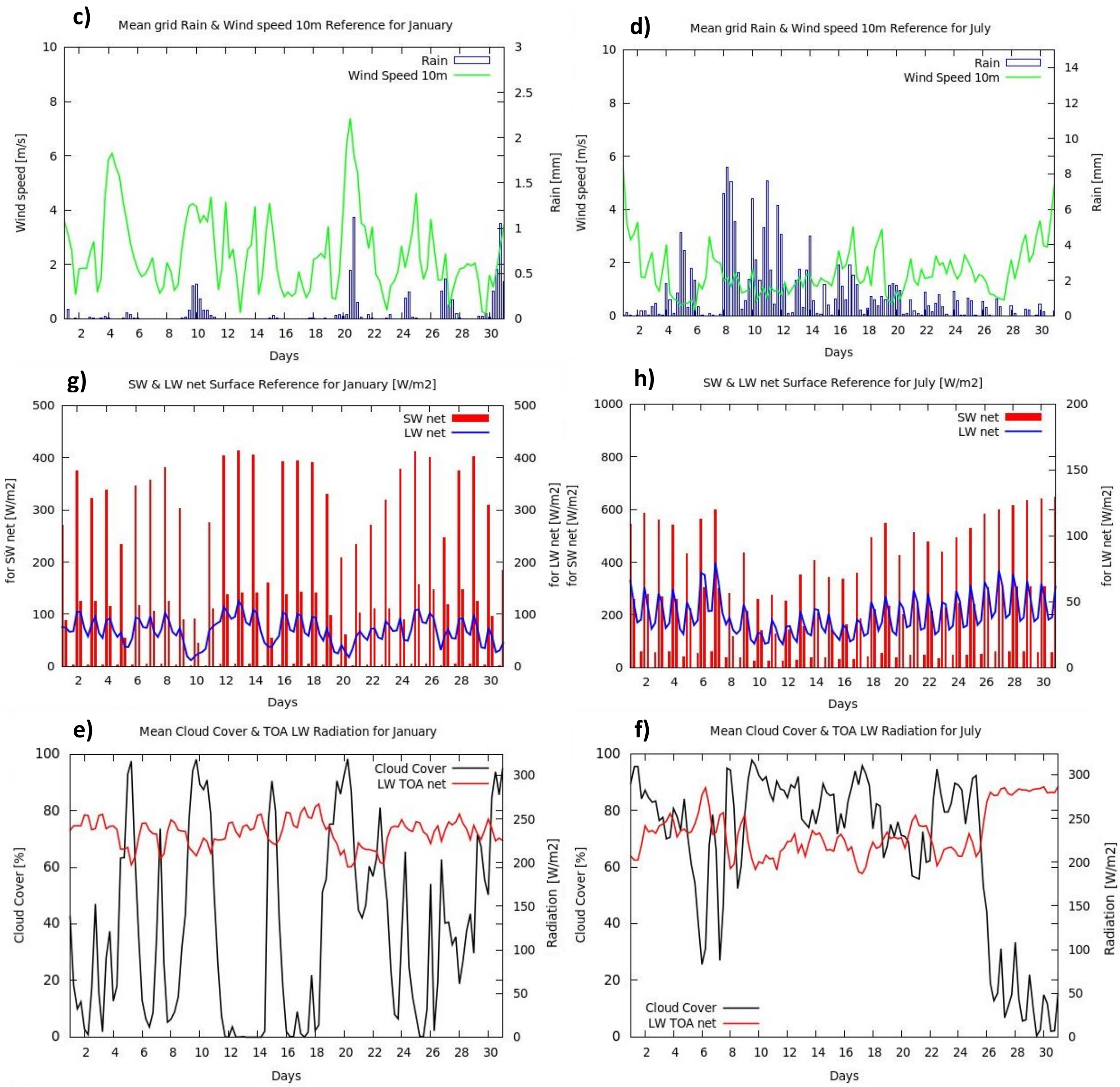

Figure 3. Average 6-hour mean land-area reference data of YRD for given parameters; 2-meter temperature and dew-point temperature displayed in ºCelsius (**a-b**), (6 hour) accumulated precipitation in the form of rain (millimetres) and total wind speed (**c-d**), fractions of Cloud Cover and net 6-hourly averaged longwave radiation at top of atmosphere (TOA, given in watts per square metre, **e-f**), net 6-hourly averaged surface long and shortwave radiation given in Watts per square meter (**g-h**). Observe scale of y-axis change for July and January cases in **a-d, g** and **h**.

For Figure 3a-b an approximation formula from Holton and Hakim (2012) was used to convert mixing ratio into dew-point temperature, approximating the 2-meter pressure over YRD to be 1013.14 hPa (global mean surface pressure). This formula is not significantly accurate, but good enough to provide an overview of the relative humidity. The net LW and SW radiation in Figure 3.e-h was converted from Jules per 6-hours over the area into watts per square metre for simplification as well. The total mean land area wind speed in Figure 3c-d is displayed as the vector sum of the mean west-east and south-north wind.

The mentioned relationship between CC, net TOA LW, net SW and LW radiation was plotted in Figure 3e-f to generally grasp in what magnitude the radiation changes through cloud cover fractions. The most distinct period of increased net TOA LW radiation from less fraction of CC is seen in the end of July, 26th to the 31st. The indirect climate effects from clouds are also roughly displayed by Figure 3a-b and 3g-h, where small elevations of surface temperature and net surface SW radiation is observed during this studied period of reduced CC.

4.1 Cloud Cover and Radiation

Comparing the total averaged land-area percentage of CC between the reference, direct and indirect aerosol cases a diagram is plotted (Figure 4) in addition to Figure 3.e-f.

a)

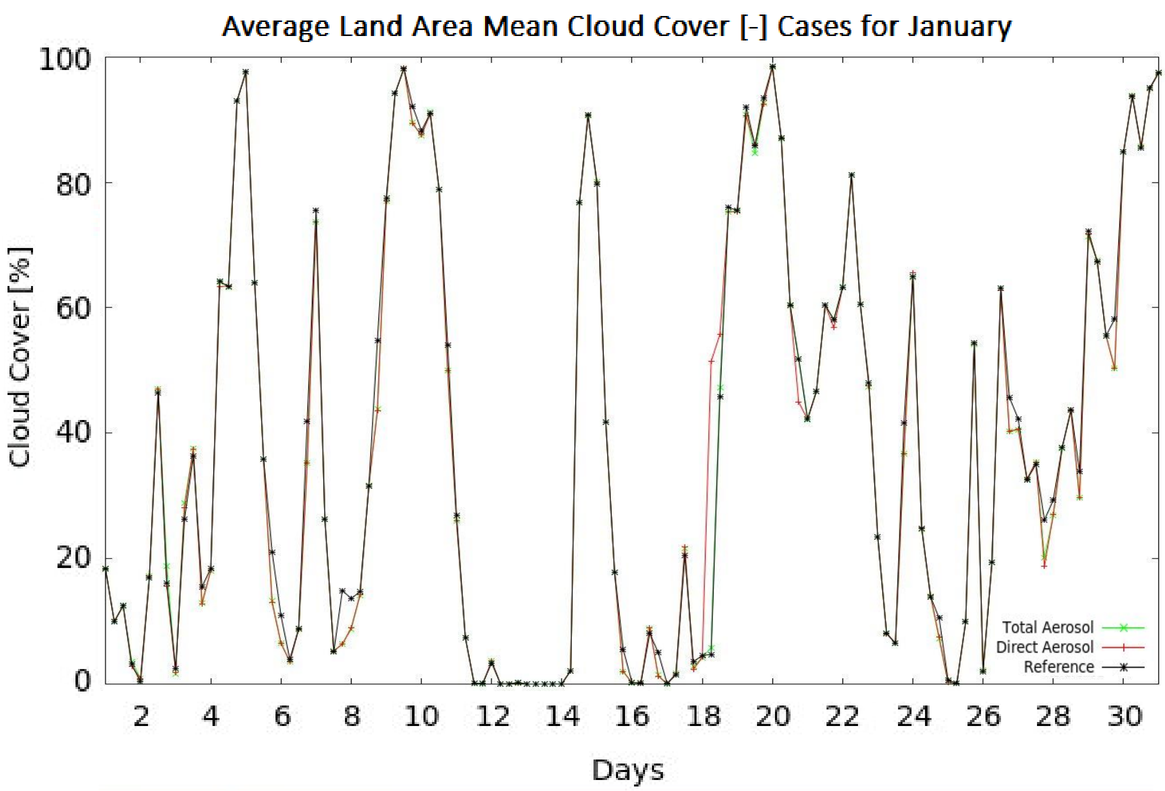

b)

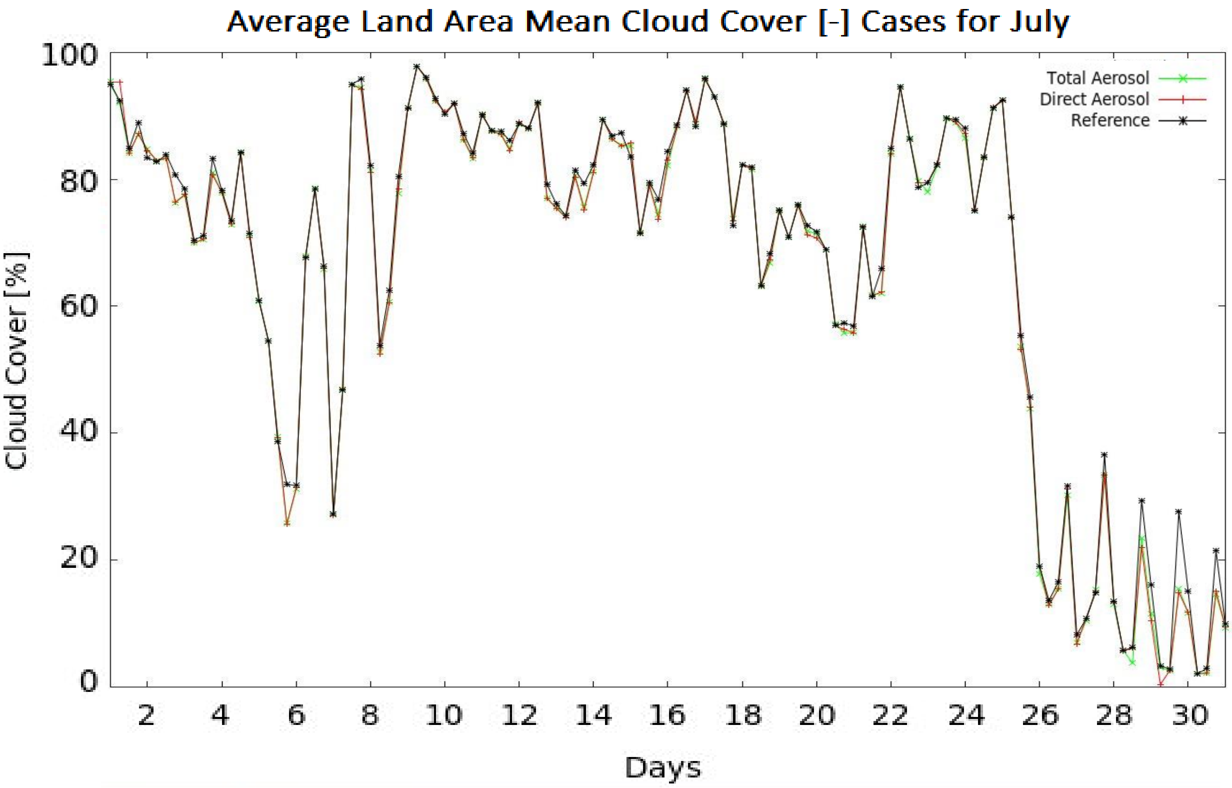

Figure 4. Land area average simulated CC percentage for the three experimental model cases over YRD for January (**a**) and July (**b**). With reference case (black), Direct Aerosol case (red) and Total Aerosol case (green).

Noticeable differences in average land area CC between the cases is only observed on few occasions, the most significant period is seen in the last days of July during daytime in Figure 4b, with a lower CC in Total and Direct Aerosol cases compared to the reference, this will investigate further in section 4.X. The calculated differences in average land area parameters is seen in Table 1 and 2.

The analysed data for cloud cover in the models were taken as snapshots and will display the amount of cloud cover at the exact time for every hourly data point, adding 6 total fractions for the main accumulated data (see Figure 5). Noted that this gives a rather inaccurate description of accumulated CC over those hours.

Plotting a two-dimensional colour map, described in Section 3, of reference model fraction of CC to correlate with the surface SW radiation maps in Figure 6.

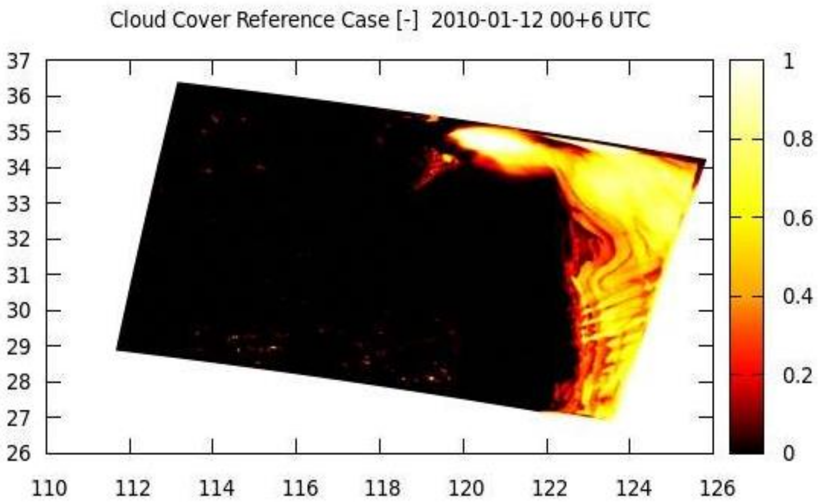

Figure 5. fraction of CC from reference case for 12th January 2010 for consecutive 00:00+6 hours UTC time, with plotted longitudes and latitudes respectively on x and y axes.

An analytic overview on the modelized surface net SW radiation output changes due to the direct climate effect in the simulated experimental models. This is Illustrated for our reference and direct aerosol case on a semi-cloud-free day, same day as figure 5. Plotting values of the two cases with a shared colour scheme on this day reveals the potential atmospheric absorption from aerosols with MACC AOD, observed in Figure 6.

a)

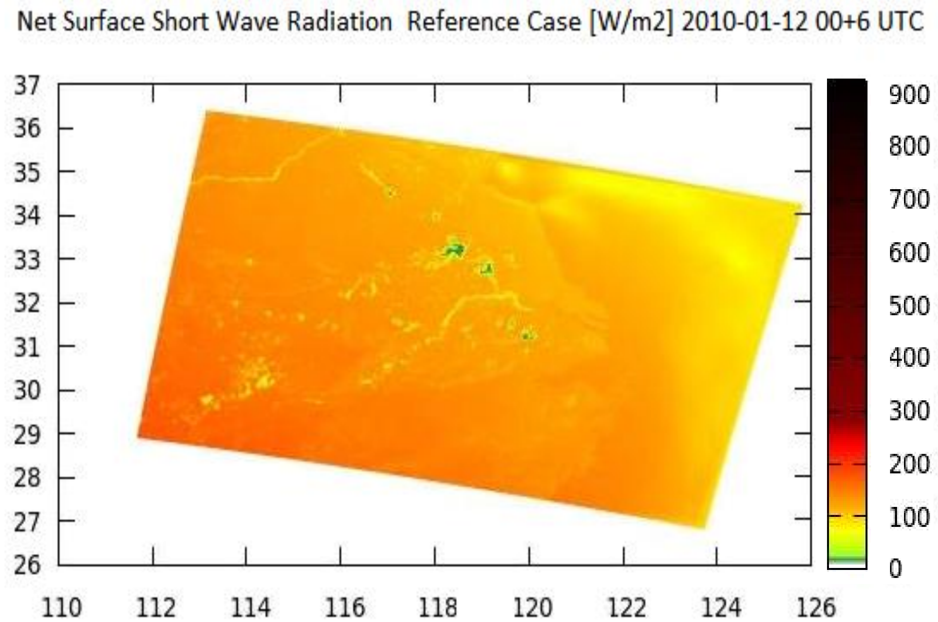

b)

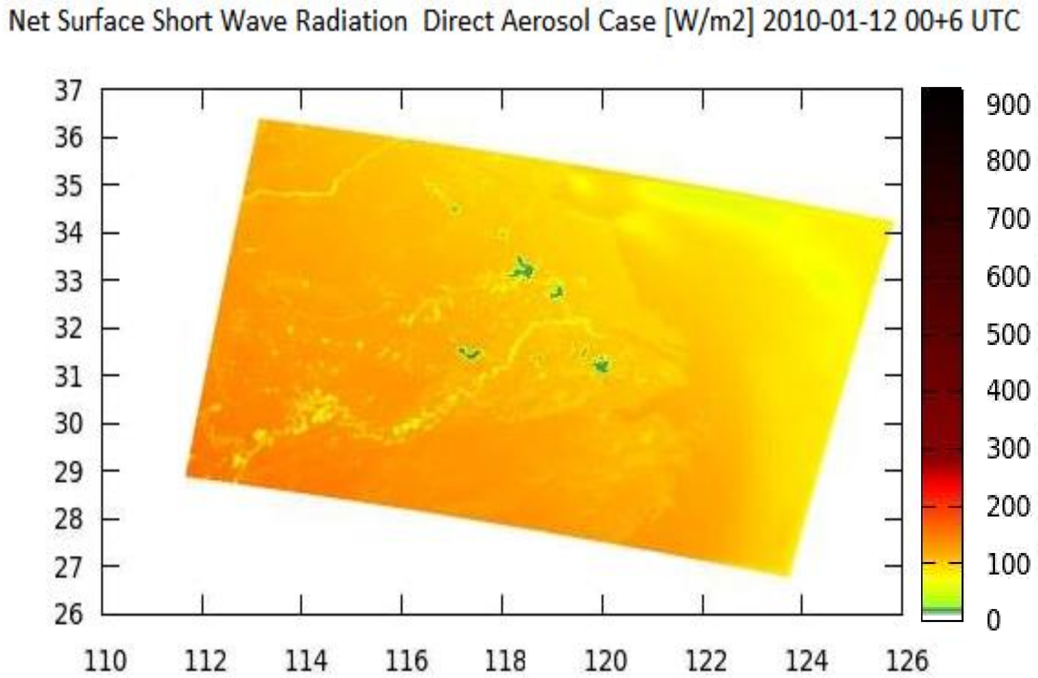

Figure 6. Net SW radiation in Reference (**a**) and Direct Aerosol (**b**) case displayed in colour-scheme as Watts per square metre on January 12th 2010 simulated over 00:00 + 6 hours UTC time, with plotted longitudes and latitudes respectively on x and y axes.

Firstly, noticeable related areas of cloud cover connected to Figure 5 over 34º North and between 122-124º West is observed in Figure 6a and 6b, where the weaker net surface SW radiation is occurring from clouds scattering the radiation and preventing solar radiation from reaching the surface, specified in Section 2.1.

Observe the case for experiment adding additional effect of the direct climate effect, seen in Figure 6.b, where general values of net SW radiation are lower when MACC-AOD aerosols are applied, implementing that some form of additional radiation absorption or scattering is occurring in the atmosphere due to increased AOD thickness.

The various albedos of land and sea areas are directly distinguishable in Figure 6.a-b, which shapes out the Chinese coastline and larger rivers in the YRD region for a nice overview. Furthermore, we comparatively reviewed net SW relations to high-density populated areas in Figure 1, but found no clear patterns connecting local changes in SW radiation to certain populated urban areas, noted that this date does not show high output of MACC aerosol fractions observed in Figure 2.

Table 1-2 and Figure 7a-b show how LW and SW radiation differs for our three experimental cases, and these two terms are added to observe the net surface radiative forcing seen in Figure 8a-b. This is performed to investigate how the different AOD and CDNC in the experimental models portrays the net radiation balance in the atmosphere.

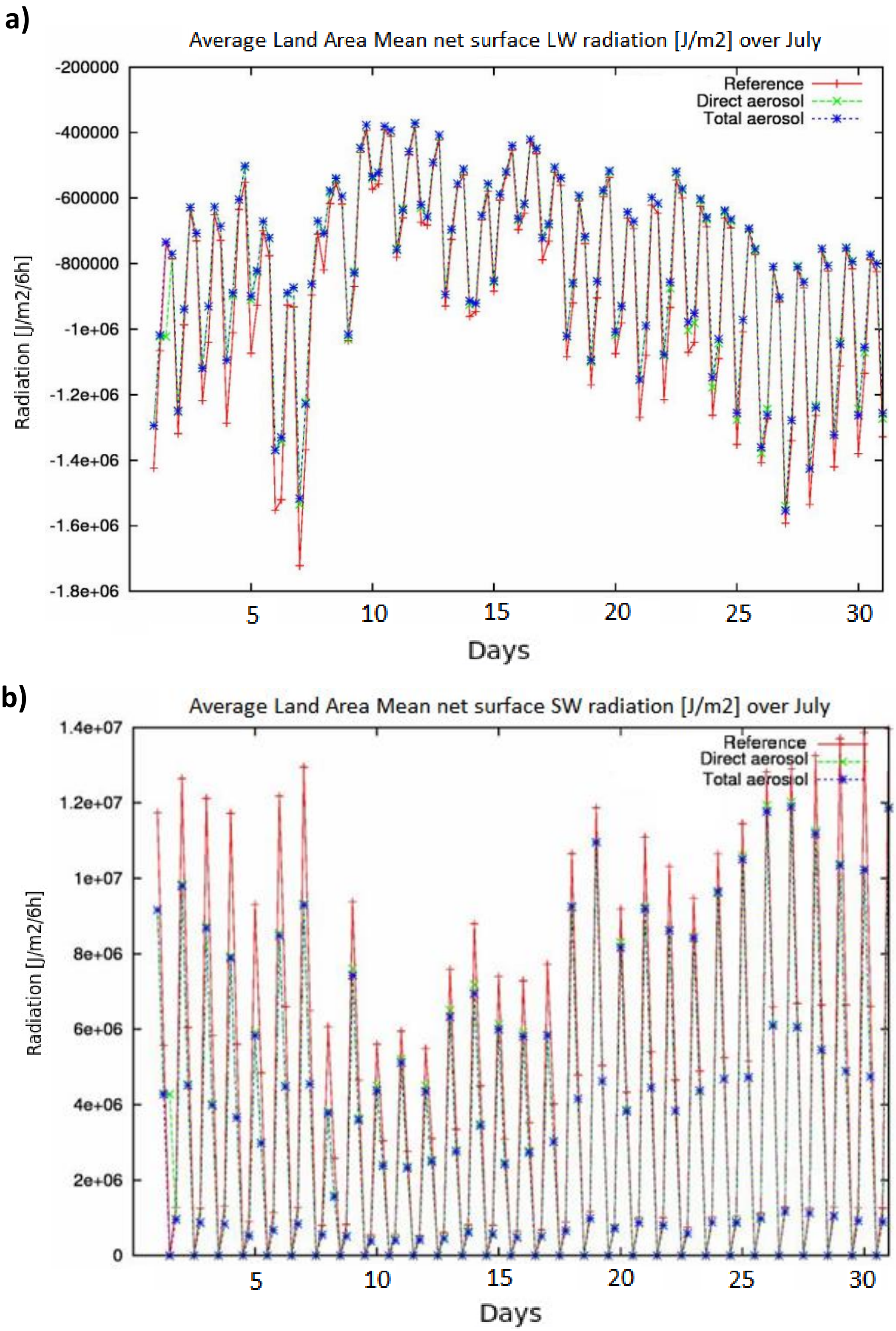

Figure 7. Average land area Net 6-hour surface LW (**a**) and SW (**b**) over July 2010 for the YRD region, with reference case (red), Direct Aerosol case (green) and Total Aerosol case (blue).

In Figure 7b, the earlier mentioned resulting effect of our MACC aerosol approximation, which increases the AOD, is observed where net SW radiation is lower for the direct aerosol model cases compared to the reference. Differences in the net surface SW radiation between the total and direct aerosol case is also distinguishable, and the mentioned Twomey effect is believed to be responsible for this further decreased amount of SW radiation reaching the surface for the total aerosol case. The difference for net SW and LW radiation is most noticeable during daytime at the accumulated 6-hourly data point 00:00+6h UTC, this is between 8 am to 2 pm local time and strongest incoming solar radiation is expected during this time.

The net surface LW radiation in Figure 7a is plotted with negative values, and the simulated total and direct aerosol cases illustrates an increased amount of surface LW radiation (negatively) compared to the simulated reference case. Yet the responsible MACC aerosol AOD effects, applying more LW radiation and added heat to the surface, is significantly smaller than the mentioned effect on SW radiation, and the results show a net positive difference at the surface from the MACC-AOD replacement of the aerosol, see Figure 8.a-f. Observe Table 1-2 for calculated values and differences between simulated experiment cases.

This difference in LW and SW radiation is dominant during the daytime 00+6h hours as seen in Figure 7a-b, and less during the night-time hours from the changes in AOD.

Converting the radiation data anew into Watts per square meter and subtracting the absolute value of the net surface LW radiation from the LW radiation, you obtain the net surface radiative balance mentioned in section 2.1, this is plotted over the YRD region for observation in Figure 8.a-f during the special case day. We observe two different times with averaged 6-hour W/m^2 to investigate local changes and to observe the direct and reference cases possible LW-SW relationship during the night, the date is used in Section 42 as a special case as well.

a)

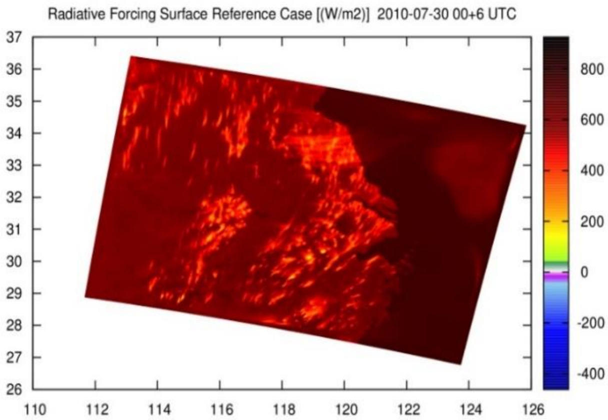

b)

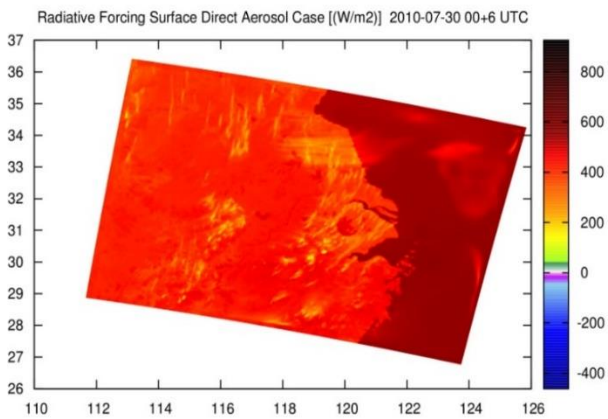

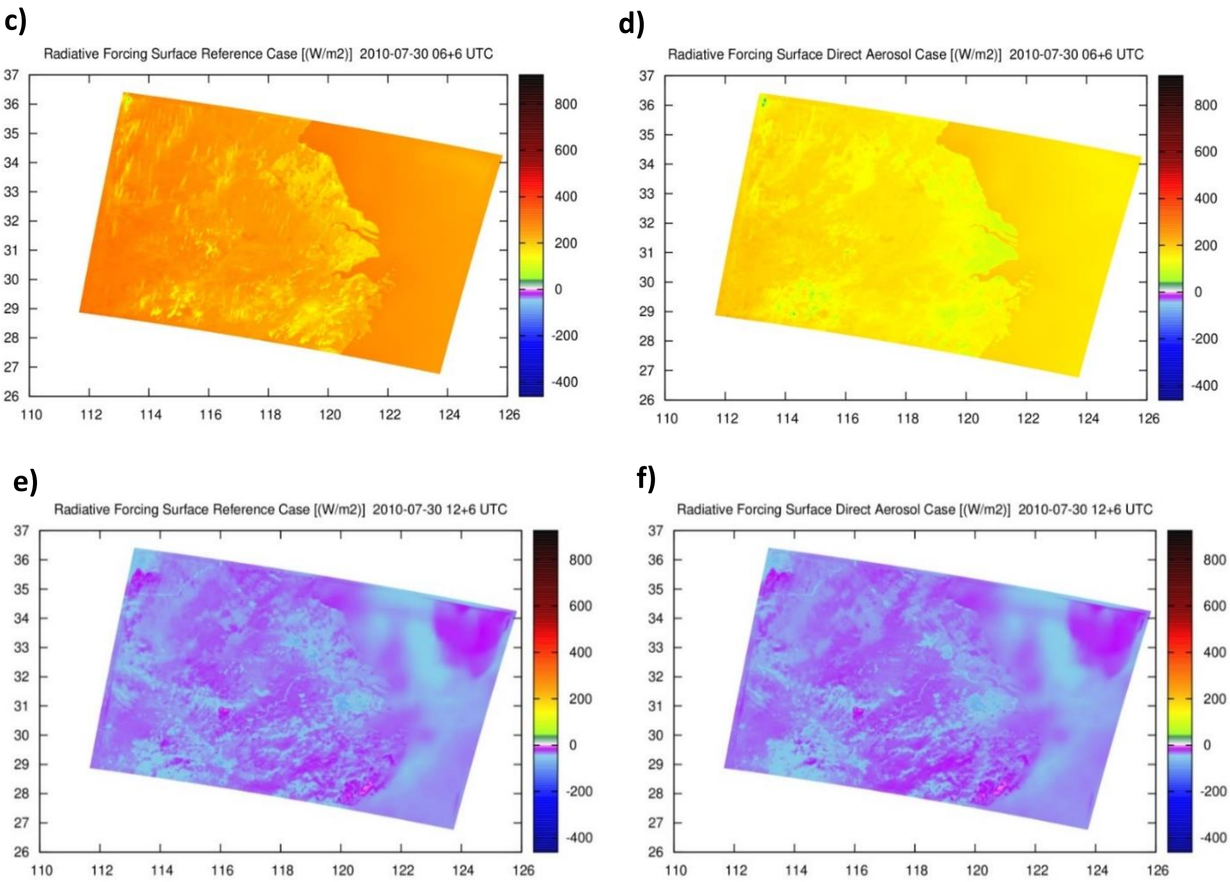

Figure 8. The net radiative (SW-LW) difference in reference (**a,c** and **e**) and direct aerosol (**b,d** and **f**) case displayed in colour-scheme as Watts per square metre on July 30th 2010 simulated and averaged over 00:00 +6 (**a-b**), 06:00 +6 (**c-d**) and 12:00 +6 (**e-f**) hours UTC time, with plotted longitudes and latitudes respectively on x and y axes. Red-black showing dominating positive (SW) radiation output and purple-blue shows dominating negative (SW) radiation output.

Figures 8a-f show clearly how the MACC aerosol AOD has it major influence during daytime hours were the two reference and direct aerosol cases have greatest differences due to the simulated direct climate effect. The mentioned opposite result from LW radiation between the cases is not distinctly seen except for a small variance seen in Figure 8e-f during night-time. These values are accumulated within the timeframe 20pm to 2am, where radiative cooling of the earth surface is observed (Figure 8d-e).

Yet, a noticeable anomaly is observed in Figure 8d over the urban region at 31º N and 121.5º W, and this additional decrease in net radiative forcing during the day, could be a local domain experiencing further climate forcing effects due to increasing anthropogenic emissions inside a highly populated urban area, as relatively high scenario of urban MACC land mean fractions are occurring this day (see Figure 2). This is however not investigated further during this study.

Table 1. Calculated averaged values of reference case parameters and differences from reference to the Total and Direct cases over YRD in January 2010, with surface temperature, CC fractions, accumulated rainfall, net surface LW and SW radiation. Difference in percentages displayed in parenthesis beneath value. Data acquired from K.P. Nielsen (2017).

January 2010	$T_{surface}$ [^{o}C]	Cloud Cover [-]	Rainfall [mm/6h]	$SW_{surface}$ [W]	$LW_{surface}$ [W]
Reference Case Average	11,49	0,390	0,0884	107,41	-64,81
Average Changes Direct Aerosol Case	-0,53 (-0,2%)	-0,004 (-1,1%)	-0,0037 (-4,2%)	-21,76 (-20,4%)	-2,31 (+3,7%)
Average Changes Total Aerosol Case	-0,54 (-0,2%)	-0,008 (-2,0%)	-0,0034 (-3,9%)	-22,69 (-20,9%)	-2,31 (+3,7%)

Table 2. Calculated averaged land area values of reference case parameters and differences from reference to the Total and Direct cases over YRD in July 2010, with surface temperature, CC fractions, accumulated rainfall, net surface LW and SW radiation. Difference in percentages displayed in parenthesis beneath value. Data acquired from K.P. Nielsen (2017).

July 2010	T surface [^{o}C]	Cloud Cover [-]	Rainfall [mm/6h]	$SW_{surface}$ [W]	$LW_{surface}$ [W]
Reference Case Average	7,67	0,664	1,22	189,35	-64,81
Average Changes Direct Aerosol Case	-0,57 (-0,2%)	-0,0080 (-1,2%)	-0,12 (-9,9%)	-36,11 (-19,2%)	-1,85 (+5,1%)
Average Changes Total Aerosol Case	-0,60 (-0,2%)	-0,0081 (-1,3%)	-0,14 (-11,3%)	-38,89 (-20,6%)	-2,31 (+5,5%)

Observing table 1 and 2, which demonstrate the monthly average mean values for the reviewed parameters over the YRD land area, confirms some of the suggested relations and is described below.

Firstly, depicting the $\frac{1}{2}$ ºC surface temperature decrease in the direct and total aerosol case, consequently due to the mentioned increase of AOD for MACC aerosols, seen in Figure 6.a-b, where the surface temperature show direct relation to the amount of net surface radiation as more surface radiation result in increasing surface temperatures. Also, the additional decrease in the total aerosol case, concerning values of surface temperature and SW radiation, occurs because of the Twomey effect. Estimating that the increasing (negatively) amount of net surface LW radiation for the total aerosol case is due to the CDNC parametrizations by Menon et al. (2002). Where applying the indirect climate effect with larger cloud optical thickness results in more LW radiated towards the surface and increasing the net LW radiation value. The studied Twomey effect relates with the given rainfall changes of the total aerosol case in Table 1-2. By resulting in further decreased amounts of rainfall, it partially confirms the mentioned phenomena where the higher CDNC prevents droplets from overcoming gravity and fall as precipitation. The Albrecht effect from Section 2.1 show no observed increase, as CC is decreasing for both aerosol cases in relation to the reference.

Connecting the decreasing amount of rainfall to observed parameter changes such as the decreased CC (about 1.2%) and elevated atmospheric SW absorption from urban aerosols (-20%), as the probable main factor of simulated reduced rainfall, brought up in Section 2.1.

However, observing values of decreased rainfall during the July (-11%) period in respect to January (-4%), could relate to the mentioned studies on anthropogenic emissions weakening the southeast-Asian summer monsoon by Bollasina et al. (2011). No further analysis on this connection was performed.

The general reduction of cloud cover in aerosol cases could be related to mentioned semi-direct climate effect stabilizing the vertical profile of the atmosphere and preventing convective cloud formation, this is also covered in Section 4.2.

4.2 July 30th Cloud Cover

This case was created to observe the hourly data sets, with accumulation and differences of CC, and mainly as follow-up investigation of the greatest case difference in CC seen in Figure 4b occurring at this date. The amount of convective clouds at these dates is significantly lower for the aerosol cases and was chosen to observe the 1-hour data sets with original snapshots of CC compared to the 6-hour accumulated snapshots to understand how big influence the reanalysed aerosols could have producing hourly forecast.

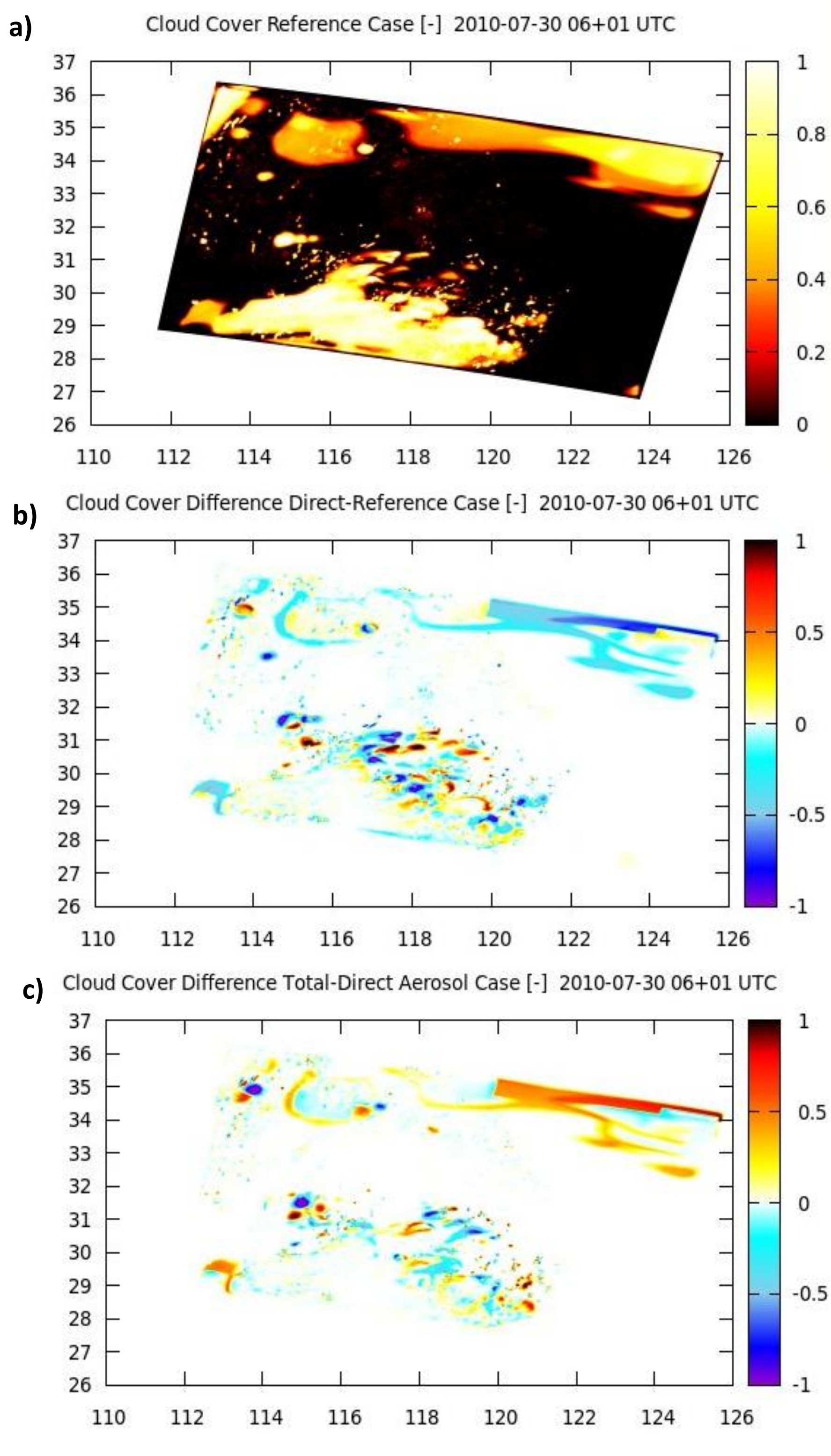

Figure 9. Fraction of CC from reference case (**a**), CC difference between Direct and Reference cases (**b**) and CC difference between Total and Direct cases (c) for 30^{th} July 2010 at 07:00 UTC time, with plotted longitudes and latitudes respectively on x and y axes.

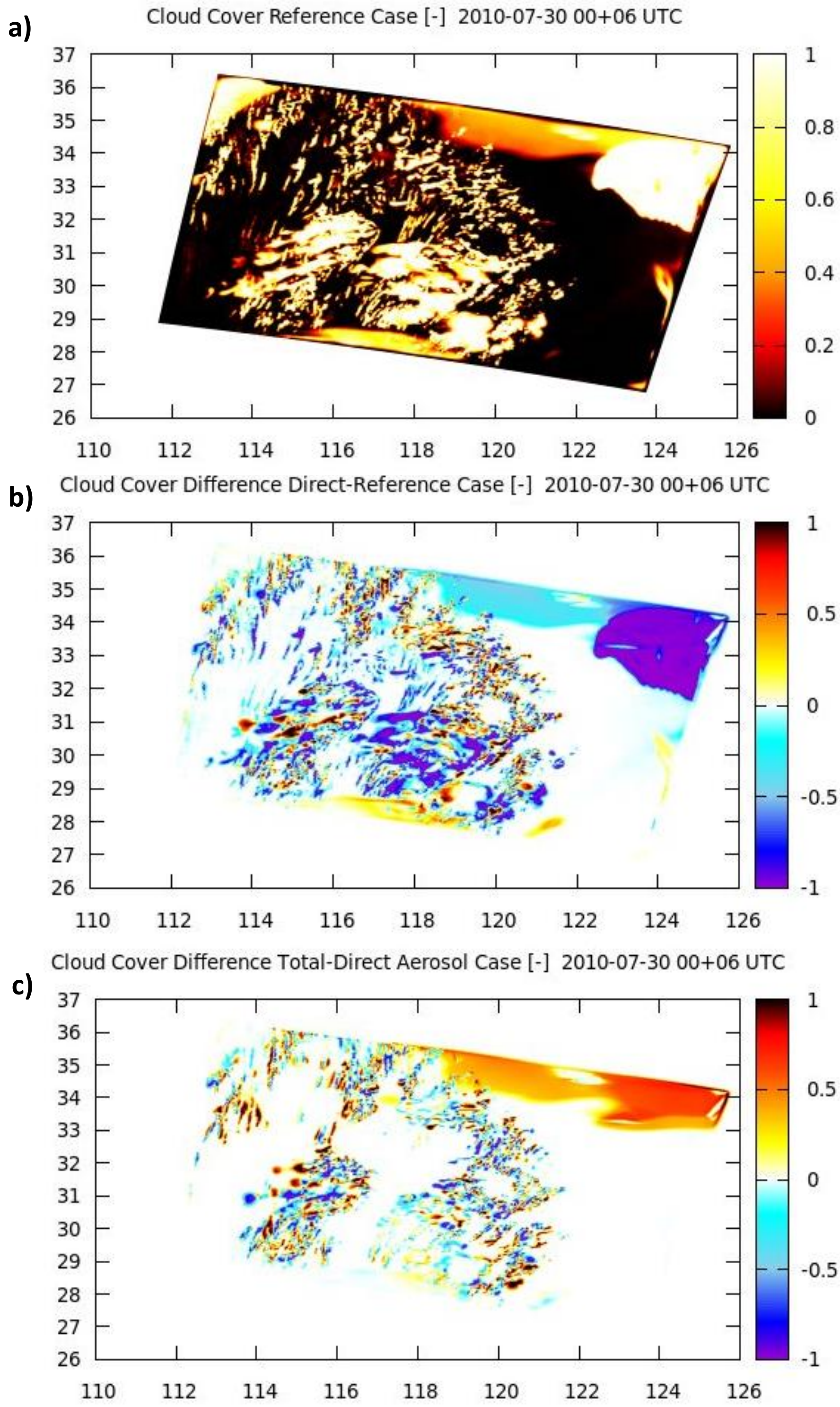

Figure 10. Fraction of CC from reference case (**a**), CC difference between Direct and Reference cases (**b**) and CC difference between Total and Direct cases (c) for 30th July 2010 hourly accumulated CC 00:00 +6h UTC time, with plotted longitudes and latitudes respectively on x and y axes.

The observed differences for our cases in Figure 9 and 10 imply a significant CC variation due to the AOD approximation, where the snapshot in Figure 9b shows how the CC differs from just one data value of one hour at 15:00 local time between the direct and reference case.

Considering that this date show relative high fractions of urban MACC aerosols, which implements that specific scenarios of greater anthropogenic emission rates during the day. This could prove some influence on the meteorological conditions related to specific days of high urban activity as studied in Wang et al. 2012. Though the other high urban MACC scenarios show fewer anomalies than July 30th.

Here the mentioned semi-direct climate effect (Wang et al. 2012) is expected to stabilize the surrounding atmosphere and be an important factor regarding the considerable decrease of convective clouds seen in Figure 10b, and in Figure 9b as well. The stabilizing effect decreases the magnitude of a possible CAPE and formation of convective clouds. The convective cloud pattern is noticeable in Figure 8 where the net surface radiative forcing is decreased by overlying CC, and possible cloud trajectory is distinguishable near the coastline in Figure 9a-c, but was not investigated further. The difference between the total and direct aerosol experiments in Figure 9c and 10c shows how the simulated total case computes more convective CC from the increased number of aerosols acting as CCN and higher CDNC. All simulated cases for each accumulated hour are displayed in appendix with the additional plots of accumulated rain-showers to observe the substantial decrease comparing direct aerosol case to the reference, yet no further research on this is made.

However, by close observation of Figure 10, the coastline over the YRD can be fairly distinguished by the formation of convective clouds due to warm near-ground moist air-parcels experiencing ascent and generating cumulus clouds, which is an elegant display from a meteorological perspective.

The atmospheric MACC AOD reanalysis models show significant decreased amount of CC and rain-showers during this day, but is not analysed in further depth, see Section 5.

5. Summary and Outlook

The direct and indirect climate effect was previously known by earlier studies on atmospheric physics and depicted by related literatures and papers in Section 2. This effect is observed through mentioned alterations in the AOD of aerosols simulated with the HARMONIE models, set to create three experimental models. These alterations were previously applied in two aerosol model cases for us to investigate and correlate studies and facts concerning the direct climate effect. Combining the AOD alterations together with a Menon et al. (2002) parametrization of CDNC, established a total aerosol case which was provided for the analytic study accounting for the indirect climate effect.

The clear relations between the new AOD and net radiation schemes is observed in Section 4.1. Evaluating how CC, surface temperatures and rain relate to the aerosols ability to perceive long and shortwave radiation, simultaneously under the influence of the indirect Twomey effects, mentioned in Section 2.

Significant CC differences between the experimental model cases in Figures 9 and 10 were observed, providing the clear analytic conclusion that by applying and experimenting with alternative aerosol characteristics in weather-modelling, you enable a more accurate NWP in regions of high anthropogenic and natural aerosol emissions, such as YRD. The 30th July case presented considerable case difference in rain-showers but was only brought through light observation.

Section 2 states that the accounted Twomey effect with increased CDNC and CCN elevates the scattering characteristics of clouds. Yet Table 1 and 2, with calculated average land area mean values, display significantly lower influence by this indirect effect compared to the resulting MACC-AOD effect from Inness et al. (2013).

But note that the actual AOD's could vary significantly in reality, and the estimated urban aerosols simulated through the models for this study implies large uncertainties in the results. This is not further explored in our analysis, as this focus study is made to understand the general relationship between simulated model aerosols and meteorological parameters.

However, studying these variations, including a vertically profiled data set, could conduct further discussion on how and where the increased urban aerosols absorb (or scatter) the SW radiation resulting in the observed greatly decreased amounts of surface net SW radiation. This case could be appealing for future studies as this input also provides an accurate stability simulation of the YRD atmosphere related to the semi-direct climate effect.

It is worth inferring that the acquired simulated experimental models for this study only include the mentioned direct, semi-direct and indirect radiative effects of aerosols. Other meteorological effects brought about by AOD alterations like drizzle formation and ice precipitation in clouds are not accounted for. Furthermore, chemical effects and cycles occurring in the atmosphere through mixing or aging of particles are not accounted for by HARMONIE weather model. and could cause altering results compared to the provided data when reacting with additional present aerosols. Example and further studies on this is done by Yu and Zhang (2011).

References

Ahrens, C.D. Meteorology Today: An Introduction to Weather and the Environment. Belmont, USA, 11th edition, 536-583. 2008.

Albrecht, B., Aerosols, cloud microphysics, and fractional cloudiness, Science, Vol.245, 1227–1230. 1989.

Bengtsson, L., U. Andrae, T. Aspelien, Y. Batrak, J. Calvo, W. de Rooy, E. Gleeson, B. H. Sass, M. Homleid, M. Hortal, K.-I. Ivarsson, G. Lenderink, S. Niemelä, K. P. Nielsen, J. Onvlee, L. Rontu, P. Samuelsson, D. Santos Muñoz, A. Subias, S. Tijm, V. Toll, X. Yang, M. Ø. Køltzow, The HARMONIE-AROME model configuration in the ALADIN-HIRLAM NWP system, Bull. Amer. Meteorol. Soc., accepted for publication, doi:10.1175/MWR-D-16-0417.1. 2017.

Bollasina, M. A., Y. Ming and V. Rawaswamy, Anthropogenic aerosols and the weakening of the South Asian summer monsoon, Science. doi:10.1126/science.1204994, 334, 501. 2011.

ECMWF, IFS documentation, European Centre for Medium Range Weather Forecasts. http://www.ecmwf.int/en/elibrary/16648- part-ivphysical-processes. 2015.

Fan, J., R. Zhang, W.-K. Tao and K. I. Mohr, Effects of aerosol optical properties on deep convective clouds and radiative forcing, J. Geophys. Res, doi:10.1029/2007JD009257, Vol.113, D08209. 2008

Holton, J. **Hakim, G.** An Introduction to Dynamic Meteorology, Volume 88, 5th edition, 58-59. 2012.

Inness, A., F. Baier, A. Benedetti, I. Bouarar, S. Chabrillat, H. Clark, C. Clerbaux, P. Coheur, R. J. Engelen, Q. Errera, J. Flemming, M. George, C. Granier, J. Hadji-Lazaro, V. Huijnen, D. Hurtmans, L. Jones, J. W. Kaiser, J. Kapsomenakis, K. Lefever, J. Leitão, M. Razinger, A. Richter, M. G. Schultz, A. J. Simmons, M. Suttie, O. Stein, J.-N. Thépaut, V. Thouret, M. Vrekoussis, C. Zerefos, and the MACC team, The MACC reanalysis: an 8 yr data set of atmospheric composition, Atmos. Chem. Phys. Vol.13, 4073–4109. 2013.

Kourtidis, K., S. Stathopoulos, A. K. Georgoulias, G. Alexandri and S. Rapsomanikis, A study of the impact of synoptic weather conditions and water vapor on aerosol–cloud relationships over major urban clusters of China. Atmos. Chem. Phys. Vol.15, 10955– 10964. 2015.

Lu, Z., Streets, D. G., Zhang, Q., Wang, S., Carmichael, G. R., Cheng, Y. F., Wei, C., Chin, M., Diehl, T., and Tan, Q.: Sulfur dioxide emissions in China and sulfur trends in East Asia since 2000, Atmos. Chem. Phys. Vol.10, 6311–6331. 2010.

Martin, G. M., D. W. Johnson and A. Spice, The measurement and parameterization of effective radius of droplets in warm stratocumulus clouds, J. Atmos. Sci. Vol.51, 1823-1842. 1994.

Menon, S., A. D. Del Genio, D. Koch and G. Tselioudis, GCM simulations of the aerosol indirect effect: Sensitivity to cloud parameterization and aerosol burden, J. Atmos. Sci. Vol.59, 692-713. 2002.

Nielsen, K.P., E. Gleeson, L. Rontu, V. Toll, Radiation Experiments and Developments, Met Eireann, Ireland, FMI, Finland, DMI, Denmark, Reading University, UK. 1, Poster. 2017

Reddy, S. M. and Boucher, O.: Climate Impact of Black Carbon Emitted from Energy Consumption in the World's Regions, Geophys. Res. Lett. Vol.34, 1-5 2006.

Stier, P., J. Feichter, S. Kinne, S. Kloster, E. Vignati, J. Wilson, L. Ganzeveld, I. Tegen, M. Werner, Y. Balkanski, M. Schulz, O. Boucher, A. Minikin and A. Petzold. The aerosol-climate model ECHAM5-HAM. Atmos. Chem. Phys. Vol.5, 1125-1156. 2005.

Streets, D. G., Gupta, S., Waldhoff, S. T., Wang, M. Q., Bond, T. C., and Yiyun, B.: Black carbon emissions in China, Atmos. Environ. Vol.35, 4281–4296. 2001

Thomas, G. E. and Stamnes, K. Radiative Transfer in the Atmosphere and Ocean, Cambridge University Press, New York, NY, USA,1st Edition, 35-53. 1999

Toll, V., Reis, K., Ots, R., Kaasik, M., Männik, A., Prank, M., and Sofiev, M. Silam, MACC reanalysis aerosol data used for simulating the aerosol direct radiative effect with the NWP model HARMONIE for summer 2010 wildfire case in Russia. Atmospheric Environment. Vol.121, 75–85. 2015.

Toll, V., Gleeson, E., Nielsen, K.P., Männik, A., Masek, J., Rontu, L., Post, P. Impacts of the direct radiative effect of aerosols in numerical weather prediction over Europe using the ALADIN-HIRLAM NWP system. Vol.172-173, 163-173. 2016.

Twomey, S. A. The nuclei of natural cloud formation. Part II: The supersaturation in natural clouds and the variation of cloud droplet concentrations. Geofis. Pure Appl. Vol.43, 227–242. 1959.

Twomey, S. A. The influence of pollution on the shortwave albedo of clouds. J. Atmos. Sci. Vol.34, 1149–1152. 1977.

Wang, W., D. Gong, Z. Zhou and Y. Guo, Robustness of the aerosol weekly cycle over Southeastern China, Atmospheric Environment. doi:10.1016/j.atmosenv.2012.07.029. 2012.

Wang, Y., Zhang, R. Y. & Saravanan, R. Asian pollution climatically modulates mid-latitude cyclones following hierarchical modelling and observational analysis. Nature Communications 5. doi:10.1016/j.atmosenv.2012.07.029. 2014.

Yu, S. and Y. Zhang, An Examination of the effects of aerosol chemical composition and size on radiative properties of multi-component aerosols, Atmos. Clim. Sci. doi:10.4236/acs.2011.12003. 2011.

Zhang, H., Z. Wang, Z. Wang, Q. Liu, S. Gong, X. Zhang, Z. Shen, P. Lu, X. Wei, H. Che, L. Li, Simulation of direct radiative forcing of aerosols and their effects on East Asian climate using an interactive AGCM-aerosol coupled system. Clim. Dyn. doi:10.1007/s00382-011-1131-0. 2011.

Picture references

SEDAC. Center for International Earth Science Information Network. Columbia University, New York. http://sedac.ciesin.columbia.edu/. (2013)

DMI logo. Accessed May 3rd 2017 at http://www.dmi.dk/om-dmi/presse/dmis-logo/

Lund university logo. Accessed May 3rd 2017 at http://www.medarbetarwebben.lu.se/

Appendix

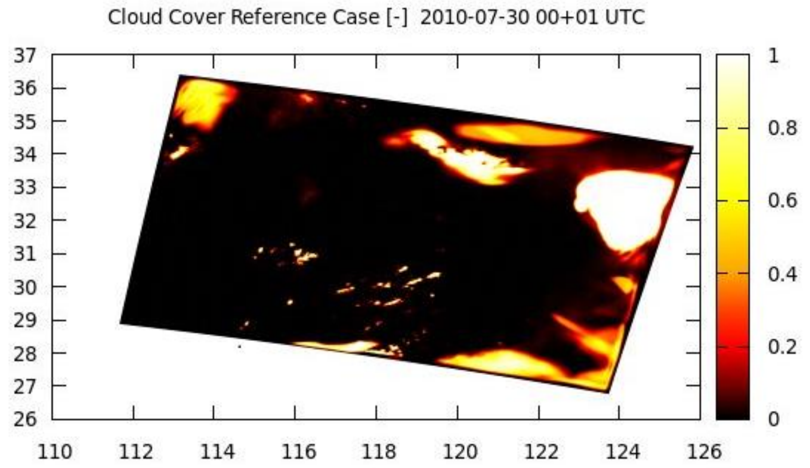

Cloud Cover Reference Case [-] 2010-07-30 00+01 UTC

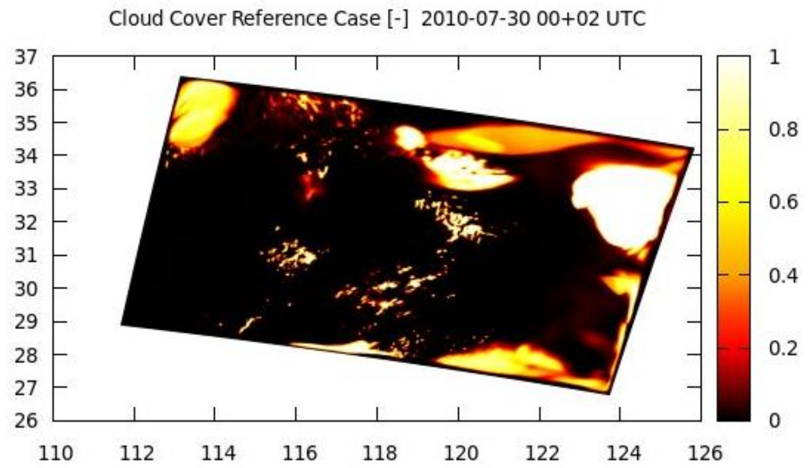

Cloud Cover Reference Case [-] 2010-07-30 00+02 UTC

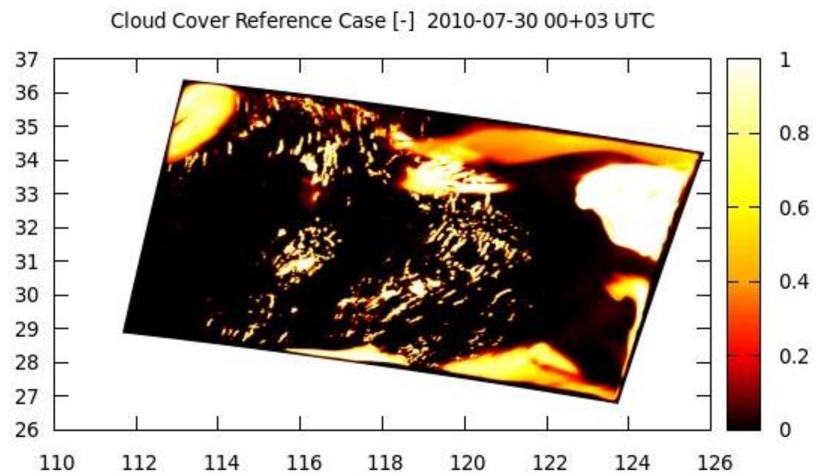

Cloud Cover Reference Case [-] 2010-07-30 00+03 UTC

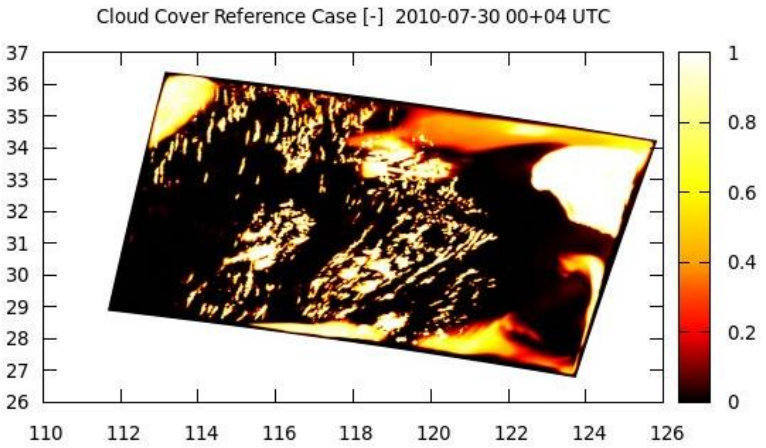
Cloud Cover Reference Case [-] 2010-07-30 00+04 UTC
37 36 35 34 33 32 31 30 29 28 27 26
110 112 114 116 118 120 122 124 126
1 0.8 0.6 0.4 0.2 0

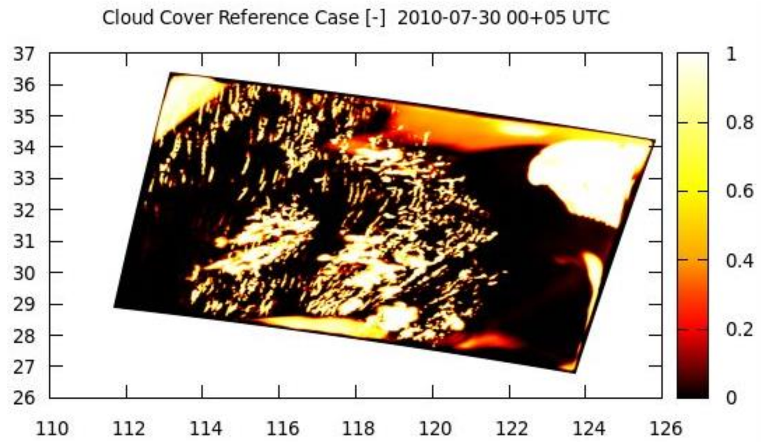
Cloud Cover Reference Case [-] 2010-07-30 00+05 UTC
37 36 35 34 33 32 31 30 29 28 27 26
110 112 114 116 118 120 122 124 126
1 0.8 0.6 0.4 0.2 0

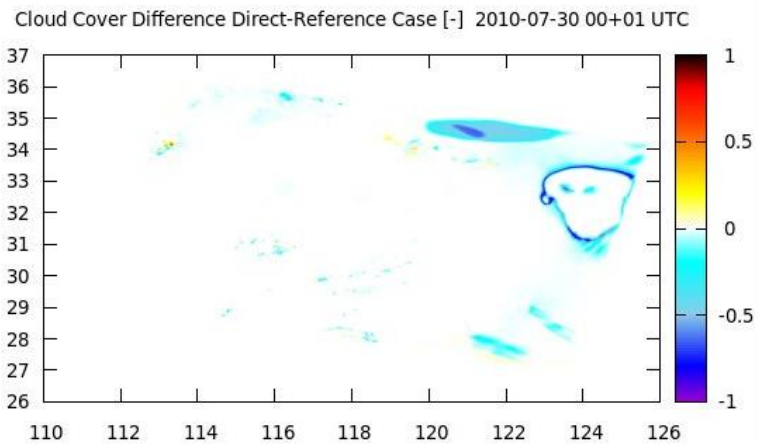
Cloud Cover Difference Direct-Reference Case [-] 2010-07-30 00+01 UTC
37 36 35 34 33 32 31 30 29 28 27 26
110 112 114 116 118 120 122 124 126
1 0.5 0 -0.5 -1

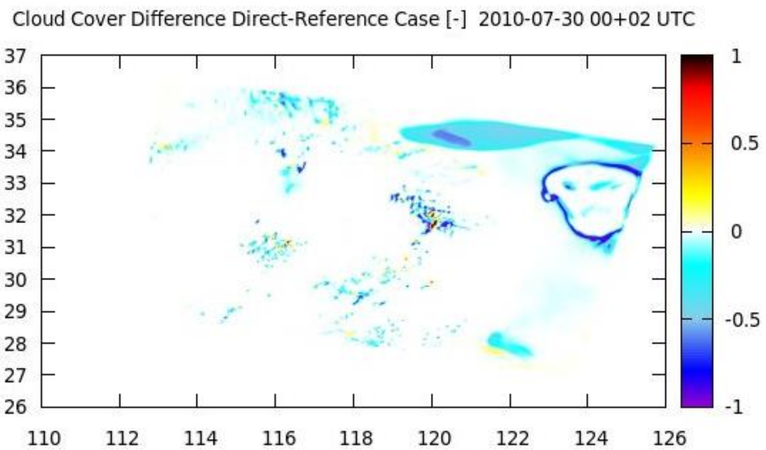
Cloud Cover Difference Direct-Reference Case [-] 2010-07-30 00+02 UTC
37 36 35 34 33 32 31 30 29 28 27 26
110 112 114 116 118 120 122 124 126
1 0.5 0 -0.5 -1

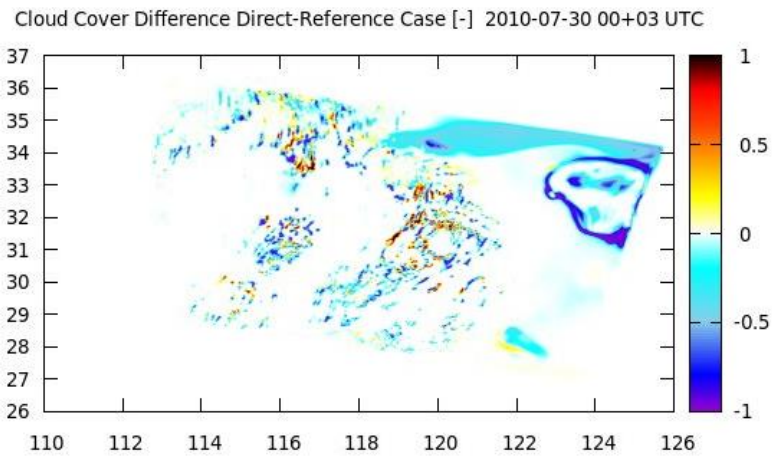
Cloud Cover Difference Direct-Reference Case [-] 2010-07-30 00+03 UTC
37 36 35 34 33 32 31 30 29 28 27 26
110 112 114 116 118 120 122 124 126
1 0.5 0 -0.5 -1

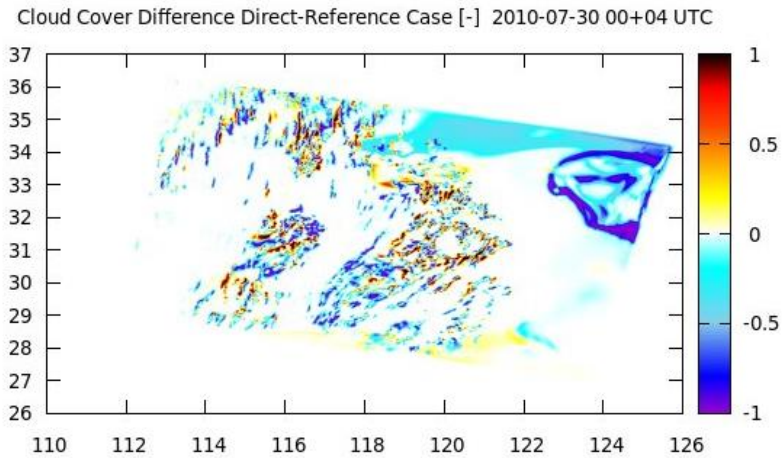
Cloud Cover Difference Direct-Reference Case [-] 2010-07-30 00+04 UTC
37 36 35 34 33 32 31 30 29 28 27 26
110 112 114 116 118 120 122 124 126
1 0.5 0 -0.5 -1

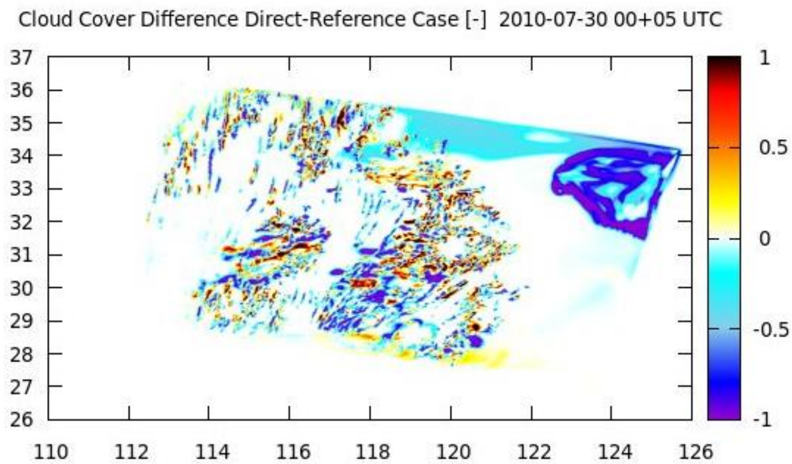
Cloud Cover Difference Direct-Reference Case [-] 2010-07-30 00+05 UTC
37 36 35 34 33 32 31 30 29 28 27 26
110 112 114 116 118 120 122 124 126
1 0.5 0 -0.5 -1

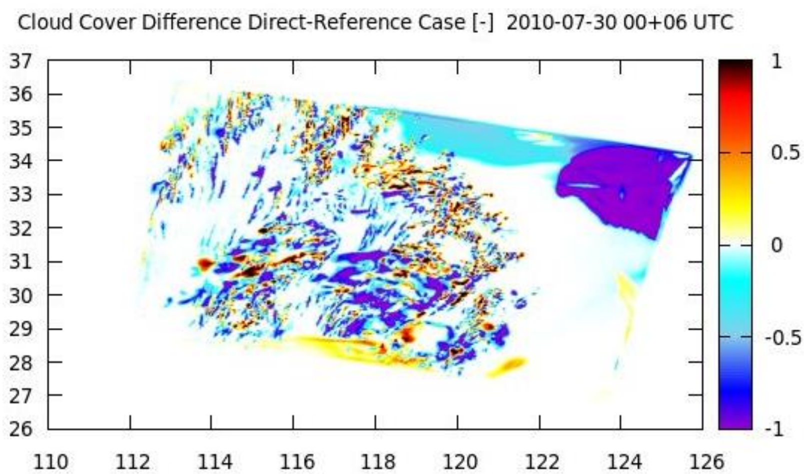
Cloud Cover Difference Direct-Reference Case [-] 2010-07-30 00+06 UTC
37 36 35 34 33 32 31 30 29 28 27 26
110 112 114 116 118 120 122 124 126
1 0.5 0 -0.5 -1

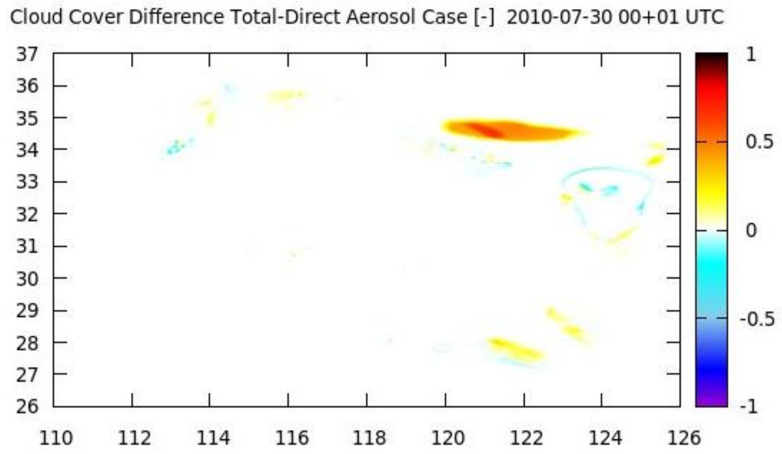
Cloud Cover Difference Total-Direct Aerosol Case [-] 2010-07-30 00+01 UTC
37
36
35
34
33
32
31
30
29
28
27
26
110
112
114
116
118
120
122
124
126
1
0.5
0
-0.5
-1

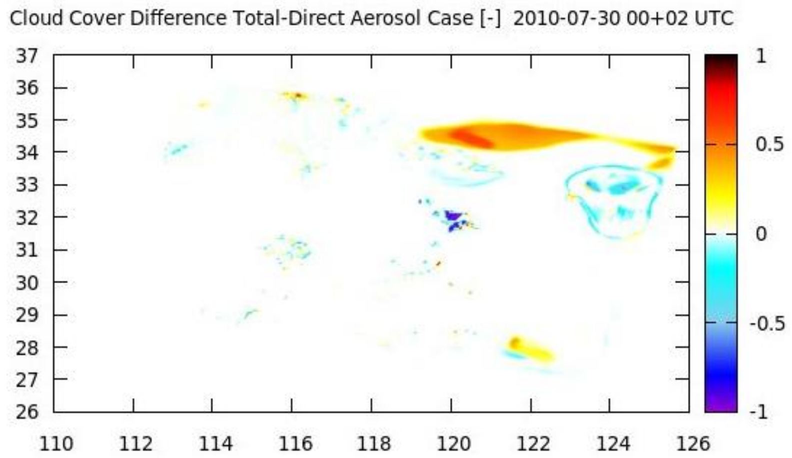
Cloud Cover Difference Total-Direct Aerosol Case [-] 2010-07-30 00+02 UTC
37
36
35
34
33
32
31
30
29
28
27
26
110
112
114
116
118
120
122
124
126
1
0.5
0
-0.5
-1

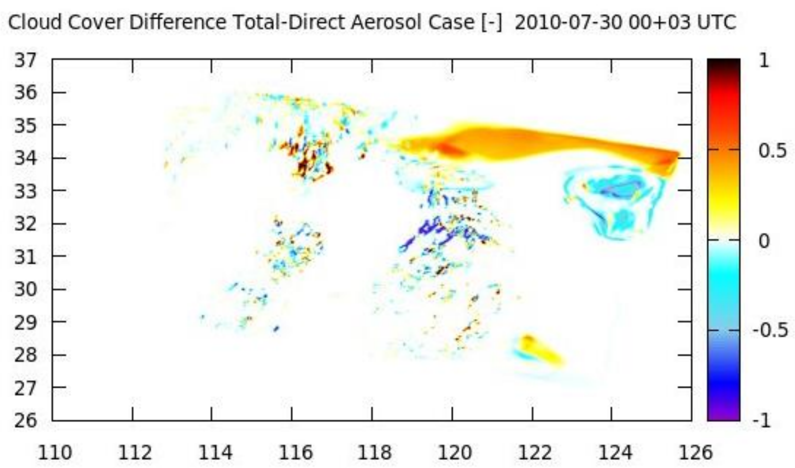
Cloud Cover Difference Total-Direct Aerosol Case [-] 2010-07-30 00+03 UTC
37
36
35
34
33
32
31
30
29
28
27
26
110
112
114
116
118
120
122
124
126
1
0.5
0
-0.5
-1

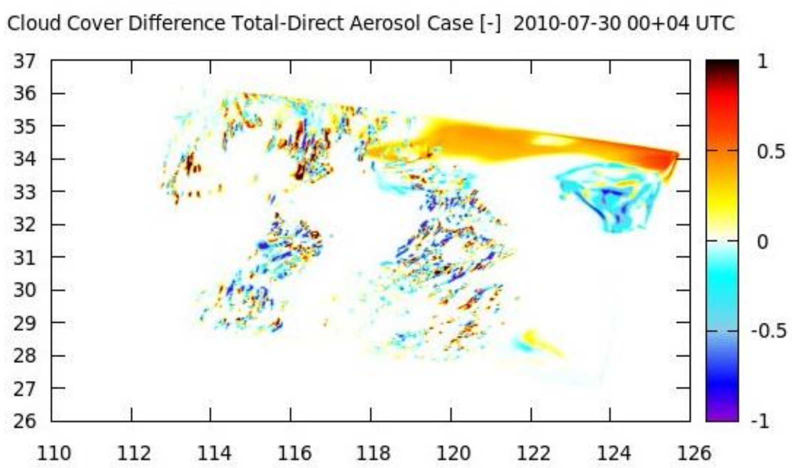
Cloud Cover Difference Total-Direct Aerosol Case [-] 2010-07-30 00+04 UTC
37
36
35
34
33
32
31
30
29
28
27
26
110
112
114
116
118
120
122
124
126
1
0.5
0
-0.5
-1

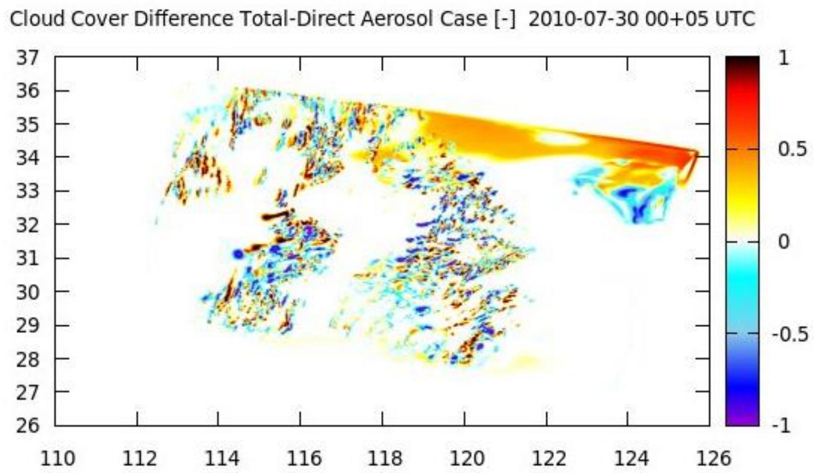
Cloud Cover Difference Total-Direct Aerosol Case [-] 2010-07-30 00+05 UTC

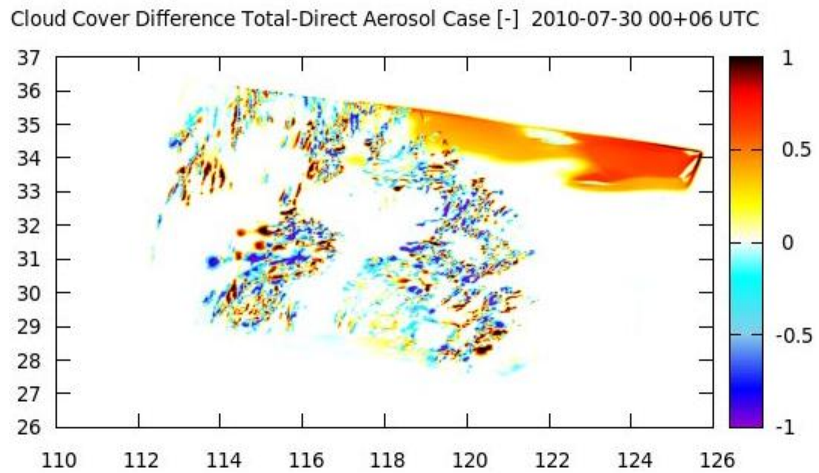
Cloud Cover Difference Total-Direct Aerosol Case [-] 2010-07-30 00+06 UTC

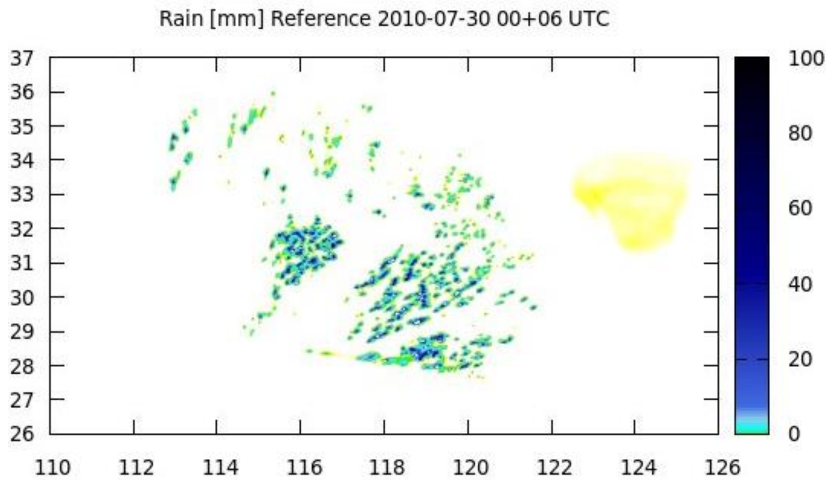
Rain [mm] Reference 2010-07-30 00+06 UTC

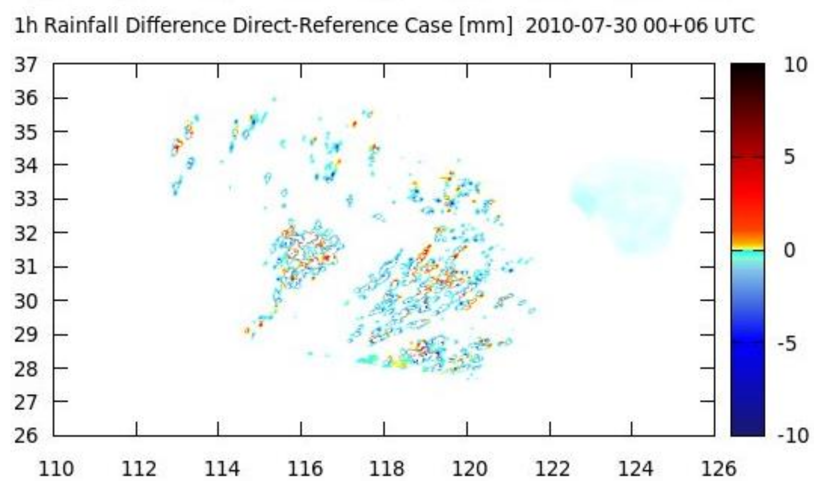
1h Rainfall Difference Direct-Reference Case [mm] 2010-07-30 00+06 UTC

Diagram Script example

```
set output
set xrange [1:31]
set yrange [0:1000]
set ylabel "for SW net [W/m2]"
set y2range [0:200]
set y2tics auto
set y2label "for LW net [W/m2]"
set xtics 2
set xlabel "Days"
set title "SW & LW net Surface Reference for July [W/m2]"
set boxwidth 0.1
set style fill solid
plot '/data/forsker8/MarcoPolo/data/Land_area_means_2010-07.dat' u ($3 +
0.042*($4)):(($32)/(6*3600)) w boxes t 'SW net' axes x1y1,
'/data/forsker8/MarcoPolo/data/Land_area_means_2010-07.dat' u ($3 +
0.042*($4)):((-$35)/(6*3600)) w l lw 2 lc rgb "blue" t 'LW net' axes x1y2,
```

Colormap Script example

```
set term postscript enhanced eps colour


set view 0,0
set zlabel ''
set cblabel ''
set pm3d map
set palette define ((-10**7)/(6*3600) "dark-blue", -(5*10**6)/(6*3600)
"blue", (-10**6)/(6*3600) "skyblue",(-4*10**5)/(6*3600) "dark-magenta",
(-10**5)/(6*3600) "violet",(-10**4)/(6*3600) "pink", 0 "white",
(8*10**5)/(6*3600) "sea-green", (1*10**6)/(6*3600) "greenyellow",
(3*10**6)/(6*3600) "yellow", (4*10**6)/(6*3600) "gold", (5*10**6)/(6*3600)
"orange", (8*10**6)/(6*3600) "orange-red", (10**7)/(6*3600) "red",
(1.2*10**7)/(6*3600) "dark-red", (2*10**7)/(6*3600) "black")

set zrange [(-1*10**7)/(6*3600):(2*10**7)/(6*3600)]
set cbrange [(-1*10**7)/(6*3600):(2*10**7)/(6*3600)]

set out
'/home/forsker8/MarcoPolo/figures/RFRWatts/Radiative_Forcing_Reference_Surf
ace_20100731_18+6.eps'
set title 'Radiative Forcing Surface Reference Case [(W/m2)]  2010-07-31
18+6 UTC'
splot '< paste /data/forsker8/MarcoPolo/data/C02_lonlats.dat
/data/forsker8/MarcoPolo/data/MarcoPolo_out_20100731_18+6.dat' u
1:2:(($30+$33)/(6*3600))  t ''
```

Loop script example for 248 figures

```
#!/bin/bash

SCRIPT_DIR=$HOME/scripts
PFILE=$SCRIPT_DIR/tmprf.plt
DATA_DIR=/data/forsker8/MarcoPolo/data
FIGURE_DIR=$HOME/MarcoPolo/figures/RFRWatts
GP_SWITCHES="-background white -alpha remove -density 400 -quality 100 -scale 50%"
YEAR=2010
for MONTH in 01 07
do
  for DAY in `seq -w 1 31`
  do
    for HOUR in 00 06 12 18
    do
       cp $SCRIPT_DIR/stemrf.plt $PFILE
       echo set out "'$FIGURE_DIR/Radiative_Forcing_Reference_Surface_${YEAR}${MONTH}${DAY}_${HOUR}+6.eps'" >> $PFI
LE
       echo set title "'Radiative Forcing Surface Reference Case [(W/m2)]  ${YEAR}-${MONTH}-${DAY} ${HOUR}+6 UTC'"
>> $PFILE
       echo splot "'< paste $DATA_DIR/C02_lonlats.dat $DATA_DIR/MarcoPolo_out_${YEAR}${MONTH}${DAY}_${HOUR}+6.dat'"
 u 1:2:\(\(\$30+\$33\)\/\(6*3600\)\)\  t "''" >> $PFILE
       Progress: $YEAR $MONTH $DAY $HOUR
       gnuplot $PFILE
       convert $GP_SWITCHES $FIGURE_DIR/Radiative_Forcing_Reference_Surface_${YEAR}${MONTH}${DAY}_${HOUR}+6.eps $FI
GURE_DIR/Radiative_Forcing_Reference_Surface_${YEAR}${MONTH}${DAY}_${HOUR}+6.jpg
       rm $FIGURE_DIR/Radiative_Forcing_Reference_Surface_${YEAR}${MONTH}${DAY}_${HOUR}+6.eps
       echo
    done
  done
done
```